Wang Lixin (Orcid ID: 0000-0003-0968-1247)

The sensitivity of satellite solar-induced chlorophyll fluorescence (SIF) to meteorological drought

Wenzhe Jiao[1], Qing Chang[2] and Lixin Wang[1]*

[1] Department of Earth Sciences, Indiana University-Purdue University Indianapolis (IUPUI), Indianapolis, IN 46202, USA

[2] Center for Spatial Analysis, Department for Microbiology and Plant Biology, University of Oklahoma, Norman, OK 73019, USA

***Corresponding author:**

Lixin Wang (lxwang@iupui.edu)

Indiana University-Purdue University Indianapolis (IUPUI)

Indianapolis, Indiana 46202, USA

Office phone number: 317-274-7764

This is the author's manuscript of the article published in final edited form as:

Jiao, W., Chang, Q., & Wang, L. (2019). The sensitivity of satellite solar-induced chlorophyll fluorescence (SIF) to meteorological drought. Earth's Future, 0(ja). https://doi.org/10.1029/2018EF001087

Abstract

Solar-induced chlorophyll fluorescence (SIF) could provide information on plant physiological response to water stress (e.g., drought). There are growing interests to study the effect of drought on SIF. However, to what extent SIF responds to drought and how the responses vary under different precipitation, temperature and potential evapotranspiration conditions are not clear. In this regard, we evaluated the relationship between satellite-based SIF product and four commonly used meteorological drought indices (Standardized Precipitation-Evapotranspiration Index, SPEI; Standardized Precipitation Index, SPI; Temperature Condition Index, TCI; and Palmer Drought Severity Index, PDSI) under diverse climate regions in the continental United States. The four drought indices were used because they estimate meteorological drought conditions from either single or combined meteorological factors such as precipitation, temperature, and potential evapotranspiration, representing different perspectives of drought. The relationship between SIF and meteorological drought varied spatially and differed for different ecosystem types. The high sensitivity occurred in dry areas characterized by a high mean annual growing season temperature and low vegetation productivity. Through random forest regression analyses, we found that temperature, gross primary production, precipitation, and land cover are the major factors affecting the relationships between SIF and meteorological drought indices. Taken together, satellite SIF is highly sensitive to meteorological drought but the high sensitivity is constrained to dry regions.

1 Introduction

Drought is one of the least understood natural hazards that can have devastating impacts on agriculture, environment and social economics in many parts of the increasingly globalized world [*Mishra et al.*, 2010; *Sheffield et al.*, 2012]. Drought occurs virtually in all climatic zones and the potential increase of drought frequency and severity due to climate change highlights the importance of a better understanding of drought to both policymakers and the scientific community [*Dai*, 2011; *Griggs et al.*, 2002; *Hao et al.*, 2017; *Van Loon et al.*, 2016].

Over the last decades, satellite remote sensing technology has been proved to be a useful tool for drought monitoring since it could provide continuous observations for drought characterizations at regional to global scales, especially for regions with limited *in-situ* observations [*Jiao et al.*, 2019; *Jiao et al.*, 2016; *Rhee et al.*, 2010; *Zhou et al.*, 2012]. Satellite observations could also be applied to estimate the drought impact on ecosystems by assessing the photosynthetic process of plants since water stress can change plants' photosynthetic capacity [*AghaKouchak et al.*, 2015]. Large-scale remotely sensed drought estimation often relies on optical, near-infrared (NIR), thermal and microwave reflectance observations. For example, satellite-based vegetation indices (VIs) have been widely used for detecting the severity and impact of drought globally through assessing the water-stress related vegetation conditions [*Asner et al.*, 2010; *Di et al.*, 1994; *Mishra et al.*, 2010; *Myneni et al.*, 1989; *Singh et al.*, 2003; *Tate et al.*, 2000; *Tucker et al.*, 1987; *Van Loon et al.*, 2016]. Some of the research indicated that VIs are good indicators to monitor drought [*Chang et al.*, 2018; *Ji et al.*, 2003; *Kogan*, 1997; *Liu et al.*, 1996; *L Zhang et al.*, 2017]. However, other studies have shown that VIs should be used with caution for drought monitoring, as they fail to capture rapid changes in drought responses since these indices are not directly linked to photosynthetic functioning [*Dobrowski et al.*, 2005; *Sun et al.*, 2015].

Solar-induced fluorescence (SIF) is the fluorescence emission from plant chlorophyll as 1-2% of the energy absorbed by chlorophyll is re-emitted at longer wavelengths as fluorescence during the light reactions process of photosynthesis [*Meroni et al.*, 2009]. In this regard, SIF is considered to have a more close relationship to the functional status of photosynthetic machinery than VIs [*Meroni et al.*, 2009]. Satellite-based SIF provides a new method for observing vegetation function from space [*Guanter et al.*, 2007; *Guanter et al.*, 2012; *Joiner et al.*, 2013; *Joiner et al.*, 2011; *Yang et al.*, 2015]. The main applications of satellite SIF products are to estimate gross primary production (GPP), light use efficiency

(LUE), vegetation photosynthetic capacity and crop productivity [*Damm et al.*, 2010; *Frankenberg et al.*, 2011; *Guan et al.*, 2016; *Guanter et al.*, 2014; *Liu et al.*, 2010; *Pérez‐Priego et al.*, 2015].

In recent years, researchers began to explore the impacts of drought on the ground observed SIF at local scales and satellite SIF at the regional scales. The results implied that SIF may have the potential to monitor the drought impacts on vegetation dynamics [*Sun et al.*, 2015; *Wang et al.*, 2016; *Yoshida et al.*, 2015]. Research indicated that SIF anomaly, which is the departure of SIF from the corresponding multiyear mean monthly value, could reasonably capture the spatial and temporal dynamics of drought severity [*Sun et al.*, 2015]. In these research work, soil moisture was used to indicate vegetation water stress and was correlated to SIF anomaly. This is because soil water deficit will lead to the closure of plant stomata and the reduction of transpiration and photosynthesis, which consequently limit plant function and decrease SIF signal [*Sun et al.*, 2015; *Yoshida et al.*, 2015]. Recent studies also indicated that site-observed SIF performs better for early drought detection compared with VIs such as Normalized Difference Vegetation Index (NDVI) [*Liu et al.*, 2018a; *Liu et al.*, 2018b]. However, the sensitivity of satellite SIF to the drought-related environmental variables is complicated and SIF anomaly is not responsive to soil water deficit alone. The change of vapor pressure deficit (VPD), LUE, fraction of photosynthetically active radiation (fPAR), and fluorescence yield under drought conditions have also been shown affecting the SIF anomaly [*Sun et al.*, 2015; *Yoshida et al.*, 2015]. In addition, SIF dynamics could be affected by some other biotic and abiotic factors such as plant functional types, temperature, and evapotranspiration [*Porcar-Castell et al.*, 2014].

Drought is a complex phenomenon which associated with multiple aspects (e.g., low relative soil moisture, precipitation deficiency, and high temperature) [*Hao et al.*, 2015]. Apart from using soil moisture to represent drought severity, meteorological drought indices, which are based on climate variables such as temperature, precipitation and potential evapotranspiration (PET), are among the most commonly used drought indices to indicate drought severity, onset, and duration. However, even if the meteorological drought indices indicate that there is a drought, the vegetation may not necessarily experience water stress and decreased SIF signal. To what extent satellite SIF responds to meteorological drought, and how the responses vary under different climatic conditions remain unclear. In this study, we characterize and quantify the relationships between GOME-2 derived 0.5° spatial-resolution SIF dataset and the four most commonly used meteorological drought indices

(Standardized Precipitation-Evapotranspiration Index, SPEI; Standardized Precipitation Index, SPI; Temperature Condition Index, TCI; Palmer Drought Severity Index, PDSI) in 3,023 counties from diverse climate regions over the continental United States (CONUS) during the growing season in the years of 2007 to 2014. We aim to address the following questions: (1) What are the spatial patterns of the relationship between meteorological drought indices and SIF anomaly in different climate regions? (2) Is there any difference in SIF sensitivity to different meteorological drought indices estimated from temperature, precipitation, and PET? (3) What are the main factors influencing the spatiotemporal patterns of the relationship between SIF and meteorological drought indices at the regional scale? (4) Under what environmental conditions satellite SIF has high correlations to meteorological drought indices?

2. Data and methodology

2.1 SIF products

Satellite measurements of SIF from chlorophyll are based on the fact that a small fraction of the energy absorbed by vegetation is emitted as fluorescence during the process of photosynthesis. The fluorescence emission has red and far-red spectrum peaks (near 685 and 740 nm) and most of the satellite SIF measurements have been in the far-red spectral region [*Yoshida et al.*, 2015]. The amount of SIF at the top-of-canopy is frequently expressed as:

$$SIF = PAR \times fPAR \times LUE_F(\lambda) \times f_{esc}(\lambda), \quad (1)$$

where PAR is the flux of photosynthetically active radiation received, fPAR is the fraction of PAR, $LUE_F(\lambda)$ can be considered as light use efficiency for SIF and $f_{esc}(\lambda)$ is the fraction of SIF photons escaping from the canopy to space. This expression of SIF is similar to LUE based GPP model and is widely used by the remote sensing community [*Sun et al.*, 2015; *Yang et al.*, 2015; *Yoshida et al.*, 2015]. There are various types of satellite SIF products with different retrieval methods: SIF derived from GOME-2, Greenhouse gases Observing SATellite (GOSAT), Orbiting Carbon Observatory-2 (OCO-2), TROPOspheric Monitoring Instrument (TROPOMI), and Scanning Imaging Absorption Spectrometer for Atmospheric Chartography (SCIAMACHY) [*Frankenberg et al.*, 2014; *Guanter et al.*, 2007; *Guanter et al.*, 2012; *Joiner et al.*, 2013; *Joiner et al.*, 2011; *Köhler et al.*, 2018; *Sun et al.*, 2018]. As SCIAMACHY derived SIF product ended in 2012, TROPOMI derived SIF product has only covered a short observation period (launched on 13 October 2017), and other

datasets could not provide a full spatial mapping of regional to global scale [*Frankenberg et al.*, 2014; *Guanter et al.*, 2016; *Köhler et al.*, 2018; *Köhler et al.*, 2015], this study only focuses on GOME-2 derived SIF product.

GOME-2 based SIF product with a spatial resolution of 0.5° latitude × 0.5° longitude (denoted as SIF hereafter) was extracted by *Joiner et al.* [2013] based on the GOME-2 data onboard the MetOp-A satellite. Level 3 of version 26 monthly product was used in this study. The GOME-2 based SIF used in this study has a morning overpass time near 09:30 local time. The detailed information about 0.5° spatial resolution GOME-2 based SIF product is available at https://avdc.gsfc.nasa.gov/pub/data/satellite/MetOp/GOME_F/.

Since most vegetation in the northern regions of the United States is dormant in the winter, our analysis focused primarily on the growing season from April to October (representing the period of active photosynthesis activities) between 2007 and 2014. During the study period, frequent drought events occurred over the CONUS. For example, in 2008 and 2009, much of south and south-central Texas experienced exceptional drought [*Nielsen-Gammon*, 2011]. California also experienced a multiyear exceptional drought which peaked in 2007-2009 and 2012-2013 [*Griffin et al.*, 2014; *Williams et al.*, 2015]. The severe drought in California also contributed to the extreme severity of the California wildfires [*Keeley et al.*, 2009]. The California drought shifted east causing large parts of Southwest and Texas suffered a harsh drought in the summer of 2011 [*Neitsch et al.*, 2011]. In 2012, much of the United States experienced one of the worst droughts in the history of the country, creating the 2012 North American drought.

2.2 Meteorological drought indices

Standardized Precipitation–Evapotranspiration Index (SPEI), Standardized Precipitation Index (SPI), Temperature Condition Index (TCI), and Palmer Drought Severity Index (PDSI) were used as meteorological drought reference data in this study. SPEI, SPI, TCI, and PDSI are among the most commonly used meteorological drought indices. SPI characterizes meteorological drought based on precipitation deficiency since it only relies on the historical distribution of precipitation to quantify the wet and dry levels [*McKee et al.*, 1993]. The SPI is simple to calculate and reflects drought conditions over different timescales and recommended by the World Meteorological Organization (WMO) as a global measure of meteorological drought [*Hayes et al.*, 1999]. TCI characterizes meteorological drought based on temperature anomaly and has been used for drought estimation by various studies

[*Bhuiyan et al.*, 2006; *Kogan*, 1995; *Kogan*, 1997; *Unganai et al.*, 1998]. SPEI characterizes meteorological drought based on the historical distribution of precipitation deficiency relative to atmospheric water demand (precipitation minus potential evapotranspiration) [*Vicente-Serrano et al.*, 2010]. SPEI has been widely used as the standard drought index by various studies for evaluating different drought monitoring methods since it is statistically robust and its multi-scalar characteristics enable identification of different drought types and impacts in the context of global warming [*Banimahd et al.*, 2013; *C Hao et al.*, 2015; *Hao et al.*, 2014; *Rajsekhar et al.*, 2015]. PDSI [*Palmer*, 1965] accounts for the balance of precipitation, temperature, and PET [*Dai*, 2011; *Wang et al.*, 2018]. Table 1 lists the detailed information about the four metrological drought indices.

Drought indices of a certain time-scale refer to the cumulative water deficit over the preceding months [*McKee et al.*, 1993; *Vicente-Serrano et al.*, 2010; *Zhao et al.*, 2017]. Different time-scales of SPI and SPEI were used in this study to explore the sensitivity of SIF to cumulative meteorological drought conditions ranging from 1 month to 12 months. Specifically, 1-, 2-, 3-, 4, 5-, 6-, 7-, 9-, and 12-month time-scale SPI and SPEI were used in this study.

The 0.5^{o} monthly raster SPI was obtained from https://climatedataguide.ucar.edu/climate-data/standardized-precipitation-index-spi; a self-calibrating version of PDSI, was obtained from http://www.cgd.ucar.edu/cas/catalog/climind/pdsi.html, and the SPEI V2.5 dataset (monthly data with 0.5^{o} spatial resolution) was obtained at http://spei.csic.es/database.html. Since daily SPEI, PDSI and SPI data covering the CONUS are not readily available, this study examines the monthly SIF responses to meteorological drought. Satellite-based TCI was calculated based on the MODIS Land Surface Temperature (LST) product (MOD11A2) using the minimum and maximum LST for each month ($TCI_i = (LST_{i,max} - LST_i) / (LST_{i,max} - LST_{i,min})$, where $LST_{i,max}$ and $LST_{i,min}$ are the maximum and minimum LST for month i from different years). Eight-day of MODIS LST was composited into monthly LST weighted by the number of days recorded in each month. MODIS LST product was obtained from the Land Processes Distributed Active Center (LPDAAC; http://lpdaac.usgs.gov/).

In this study, we used the county as the basic geographic unit to reduce the effect of low-quality SIF data or missing SIF observations in some pixels on our assessments. We excluded urban, barren and water dominated counties and focused on 3,023 vegetation covered counties in our study. In the county-level statistics, given that some small counties

are smaller than the smallest grid cell for the raster SIF data and some large counties in the west may contain multiple grid cells, we divided each SIF grid cell into 10,000 small grid cells without changing the value, then we used the mean value of these small grid cells located in the corresponding counties to represent the county value. The mean SPEI, SPI, TCI and PDSI values were also calculated for each county. In order to evaluate the sensitivity of satellite SIF to meteorological drought at the county level, we firstly calculated the mean SPEI, SPI, TCI and PDSI values in each county, then correlated these values to the mean SIF anomaly values in each county. We compared the sensitivity of SIF for each over the CONUS.

2.3 Ancillary data

In order to investigate the factors modulating the sensitivity of the satellite SIF to meteorological drought as comprehensive as possible, ten additional datasets were used as the explanatory covariates to explain the spatial variations in the relationships between satellite SIF product and meteorological drought indices. These additional datasets include climate data (historical mean annual growing season temperature and historical mean annual growing season precipitation), land use and land cover (LULC) data, historical mean annual growing season vegetation gross primary production (GPP), digital elevation model (DEM) data and soil property data (soil permeability, hydrology group, water holding capacity and soil drainage).

In this study, LULC information in each county was obtained from National Land Cover Database 2011 (NLCD 2011), which are available at the U.S. Geological Survey National Land Cover Data (NLCD) Institute (http://landcover.usgs.gov/). The majority of the land cover pixel was used to represent the county's LULC type. Each county's majority LULC type was calculated using Zonal statistical function in the ArcGIS software. Counties with LULC types of non-vegetation were excluded. The gridded historical mean annual precipitation was calculated for each county using seven years (2007-2014) growing season (April to October) data obtained from the Oregon State University PRISM group (http://prism.oregonstate.edu). Mean annual temperature in each county was obtained using 2007-2014 growing season (April to October) MODIS land surface temperature (LST, MOD11A2, with 8-day temporal resolution and 1-km spatial resolution) data. Mean value of the gridded time series of MODIS LST was calculated for each county. For vegetation data, we calculated the mean annual GPP using MODIS GPP product (MOD17A2, with 8-day

temporal resolution and 1-km spatial resolution) for the growing season from the year of 2007-2014. Detailed information about these vegetation and land surface temperature datasets are available at https://modis.gsfc.nasa.gov/data/. Gridded DEM for each county is obtained using Space Shuttle Radar Topography Mission (SRTM) product. Soil properties (permeability, water table depth, available water holding capacity, hydrologic groups, and soil drainage) in each county were derived from the STATSGO soil database which was downloaded from the Center for Environmental Informatics at Pennsylvania State University (http://www.soilinfo.psu.edu/). The mean value of the gridded precipitation, temperature, GPP and soil data was used to represent the county's precipitation, temperature, GPP and soil properties. Similar with LULC data, each county's mean precipitation, temperature, GPP, and soil property values were calculated using Zonal statistical function in the ArcGIS software.

2.4 Calculation of SIF anomaly

The z-score was used to represent the anomaly of GOME-2 SIF data from 2007 to 2014. The z-score of SIF anomaly was calculated as

$$A_{j,i} = \frac{SIF_{j,i} - \overline{SIF_j}}{\sigma}, \quad (2)$$

where $A_{j,i}$ denotes SIF anomaly for the month j in year i. $\overline{SIF_j}$ denotes the averaged SIF of month j over the year 2007-2014; σ is the standard deviation of SIF for month j over the year 2007-2014. The SIF anomaly was compared with SPEI, SPI, TCI and PDSI in different counties across the CONUS. The Spearman rank correlation coefficients (r-values) between the SIF anomaly and four meteorological drought indices (SPEI, SPI, TCI, and PDSI) were used to evaluate the sensitivity of satellite SIF to the meteorological drought conditions in this study. High correlation coefficients indicate high sensitivity and *vice versa*.

2.5 Random forest regression

In order to quantify the factors modulating the sensitivity of the satellite SIF to meteorological drought, the random forest regression model was used to examine the relationship between the satellite SIF drought sensitivity and explanatory covariates. Random forest regression is a non-parametric statistical method requiring no distributional assumptions on covariate in relation to the response variable [*Breiman*, 2001]. The random forest algorithm here uses 1000 binary decision trees. In standard trees, each node is split using the best split among all variables. The explanatory covariates used are: historical mean annual growing season temperature, mean annual growing season precipitation, LULC, mean

annual growing season GPP, DEM, mean soil moisture, soil permeability, hydrology group, water holding capacity, and soil drainage. With the random forest regression model, variable importance ranking for variable selection was also calculated. The variable importance measures how much the error increases if we scramble the values of a variable. Larger error before and after permutation means larger importance of the variable in the forest and contribute more to predictive accuracy than other variables [*Breiman*, 2001].

3 Results

3.1 Temporal and spatial patterns of the correlations between SIF and meteorological drought indices

The SIF anomalies were compared against each of the four meteorological drought indices, specifically: PDSI, TCI, SPI (1-, 2-, 3-, 4-, 5-, 6-, 7-, 9- and 12-month time-scales) and SPEI (1-, 2-, 3-, 4-, 5-, 6-, 7-, 9- and 12-month time-scales) in all 3,023 counties across the CONUS. SIF has the highest correlation with PDSI (r =0.257) followed by TCI with a similar value (r=0.249). SIF has similar correlations with SPI and SPEI under different time-scales and the correlations were generally lower than those with PDSI and TCI. Over the CONUS, there was significant spatial variability in the correlations between satellite SIF and SPEI, the r-values ranged from -0.4 to 0.9 (Figure 1). This was similar to the correlation ranges between satellite SIF and SPI (Figure 2), TCI, and PDSI (Figure 3). Generally, SIF showed similar spatial variability and their correlations with different meteorological drought indices of different time-scales were uniform (Figures 1-3). There were much stronger positive correlations between SIF and meteorological drought indices in the counties in the middle CONUS than counties in the eastern and western CONUS. For example, for the r-values between SIF and SPEI-3, SPI-3 and PDSI (denotes as $R_{SIF\text{-}SPEI03}$, $R_{SIF\text{-}SPI03}$, and $R_{SIF\text{-}PDSI}$) in Figures 1-3, many of the counties in the southwestern CONUS (e.g., some counties in Nevada, California, and Arizona) had $R_{SIF\text{-}SPEI03}$, $R_{SIF\text{-}SPI03}$ and $R_{SIF\text{-}PDSI}$ close to zero and p-value > 0.05, whereas most counties in the north-central and south-central CONUS (e.g., counties in Texas, Oklahoma, Kansas, Dakota, and Nebraska) had $R_{SIF\text{-}SPEI03,}$ $R_{SIF\text{-}SPI03}$ and $R_{SIF\text{-}PDSI}$ exceeding 0.75 and p-value <0.05. Besides the significant positive correlations in the middle of CONUS, there are significantly negative correlations between SIF and meteorological drought indices mainly in the Pacific Northwest and Northeast regions.

Vegetation across the CONUS is susceptible to both energy and water constraints. The relative importance of these constraints differs along climate gradients and vegetation

water sensitivity also likely varies for different plant functional types. To this end, we evaluated the sensitivity of SIF to metrological drought for different ecosystem types. Figure 3 (b) and (d) show the correlations between SIF and PDSI as well as between SIF and TCI, respectively, for different ecosystem types. Generally, SIF had higher positive correlations with PDSI and TCI for grassland and shrubland ecosystems than other ecosystem types. Most of the grassland and shrubland ecosystems only had positive correlations with PDSI and TCI. SIF had lowest positive correlations for deciduous and evergreen forests than other ecosystem types. The sensitivity of SIF to the meteorological indices of different ecosystem types were also different for different time-scales (Figures 4 and 5). Pairwise t-test indicated that there were significant differences of the positive r-values between crop SIF and 1- to 4-month time-scale SPEIs, but there was no significant difference for the negative correlations. Deciduous forest and evergreen forest responded to different meteorological drought time-scales differently. Deciduous forest SIF did not show significantly different correlations when correlated to SPEI from 2-month to 12-month time-scales, while the positive r-values of evergreen forest SIF and 1-, 2-, 3-, 7-, 9-, and 12-month SPEIs showed significant differences (p-value <0.05 in pairwise t-test). Within the 1-, 2-, 3-, 7-, 9-, and 12-month time-scales, along with the increasing time-scales, mean r-values between evergreen SIF and SPEIs became higher. Grassland SIF had only positive correlations for all the time-scales of SPI and 2 to 12-month time-scales of SPEI. Comparing with different drought time-scales, grassland SIF had highest correlation to 3-month SPEI and longer term of meteorological drought did not significantly change grassland SIF sensitivity (Figure 4). Shrubland SIF had both positive and negative correlations with SPEI for the time-scale of 1 to 5 months and only positive correlations for the time-scale of 6 to 12 months. The positive correlations between shrubland SIF and SPEI increased when SPEI time scales increased from 1-month to 4-month. However, different from other ecosystems, there was a decrease of mean positive r-values when shrubland SIF correlated to SPEIs ranging from 6-month to 12-month time-scales. We found similar patterns of SIF sensitivity to different time-scales of SPI. The only exception is that there was different relationship of wetland SIF to SPEI and SPI. There was no significant difference between wetland SIF and SPIs for different time-scales but SPEI with time-scales longer than 4-months had higher positive correlations with wetland SIF.

3.2 Driving forces of the observed spatial variability

To examine the driving forces of the observed spatial variability in the relationships between the SIF anomaly and meteorological drought indices, ten independent variables

(described in section 2.3) were evaluated using random forest regression. Because of the similar spatial variability and magnitude in correlation coefficients between SIF and those meteorological drought indices of different time-scales, we chose to focus on the relationships between the SIF and SPEI-5, SPI-5, TCI and PDSI in our analysis.

All the variables together explained 77.76% of the variation in the r-value between SIF and SPEI-5 (denotes as $R_{SIF\text{-}SPEI05}$). In comparison, these ten independent variables explained 77.56%, 78.49%, and 78.68% of the variations in the r-values between SIF and SPI-5 ($R_{SIF\text{-}SPI05}$), between SIF and TCI ($R_{SIF\text{-}TCI}$), and between SIF and PDSI ($R_{SIF\text{-}PDSI}$), respectively. The variable importance function in the random forest model was used to quantify the rank of how each variable modulates the variance of $R_{SIF\text{-}SPEI05}$, $R_{SIF\text{-}SPI05}$, $R_{SIF\text{-}TCI}$ and $R_{SIF\text{-}PDSI}$. Figure 6 shows the rank of importance for the ten independent variables controlling the sensitivity of SIF to meteorological drought. Figure 6 shows each variable on the y-axis, and their importance on the x-axis, ordering from top-to-bottom as most to least important. The variable importance (x-axis value in Figure 6) is the difference in 'Out of Bag' [*Breiman*, 1996] prediction error before and after permutation. A larger variable importance value indicates that misspecification detracts from the predictive accuracy in the forest. Smaller variable importance value indicates the variable contributes less to the predictive accuracy [*Ishwaran*, 2007].

The results showed that mean annual temperature was the most important variable in explaining the spatiotemporal distributions of r-value distributions (Figure 6). Less important but still of major influence was the mean annual growing season GPP. Mean annual growing season precipitation was the next significant variable. Compared with the factors described above, DEM, LULC and the soil conditions (soil drainage class, organic material, permeability, water holding capacity, and hydrologic group) were the less significant variables affecting the $R_{SIF\text{-}SPEI05}$ distributions. Similar to $R_{SIF\text{-}SPEI05}$, temperature appeared to be the most dominant driver for the spatial distribution of $R_{SIF\text{-}SPI05}$, $R_{SIF\text{-}TCI}$ and $R_{SIF\text{-}PDSI}$. Mean annual GPP and precipitation were the next top significant variables associated with the strength of $R_{SIF\text{-}SPI05}$, $R_{SIF\text{-}TCI}$ and $R_{SIF\text{-}PDSI}$. LULC was the fourth important factor. Also, DEM and the soil conditions were the less significant variables (Figure 6).

To demonstrate an environmental envelope for the sensitivity of satellite SIF to meteorological drought and show areas of high SIF sensitivity to meteorological drought, Figure 7 displays the dependence of SIF and meteorological drought index correlation on the top three independent environmental variables across a wide range of observed values. Since

PDSI, TCI, different time-scales of SPI and SPEI showed similar spatial variability and their correlations with SIF anomaly were uniform (Figure 1-3), we focused on the relationship between SIF anomalies and SPEI-5. The black points with p-value < 0.05 indicate the points with a statistically significant relationship between SIF and SPEI-5.

In Figure 7, the blue and brown lines represent the thresholds of 90% and 80% of the counties with a significant correlation between SIF and SPEI-5, respectively. That is, for example, for the counties with mean annual growing season temperature higher than the blue line (i.e., >30.6°C), the percentage of counties with significant correlations between SIF and SPEI-5 (black points in Figure 7a) is more than 90% (all the points at the right side of the blue line in Figure 7a). That is, satellite SIF anomaly was sensitive to meteorological drought for areas with mean annual growing season temperature higher than 30.6 °C. Similarly, regions with mean annual growing season GPP less than 750 g C m^{-2} yr^{-1} or mean annual growing season precipitation less than 700 mm were areas with high sensitivity of satellite SIF to meteorological drought. Figure 7d) -7f) displayed the suggested suitable areas for using satellite SIF to characterize meteorological drought based on 80% threshold in mean annual growing season temperature, GPP, and precipitation. Supplemental materials Figures S1 to S6 showed the detailed correlations between SIF and all the ten environmental variables.

4 Discussion

4.1 SIF sensitivity to different climate variables

The correlation of SIF to meteorological drought indices not only reflects SIF response to drought stress but also reflects the sensitivity of SIF to different climate variables. For example, SPI is only based on the historical distribution of precipitation and high SPI could indicate wet conditions. Therefore, the correlation between SIF anomaly and SPI could potentially reflect the sensitivity of SIF to precipitation dynamics. Similarly, TCI is only based on temperature variable, the correlation between SIF anomaly and TCI could potentially indicate the sensitivity of SIF to temperature variations. SPEI represents meteorological drought using the combination of precipitation and PET. The correlation between SIF anomaly and SPEI indicates the sensitivity of SIF to the dynamics of precipitation deficiency relative to PET. Similarly, the correlation between SIF anomaly and PDSI indicates the sensitivity of SIF to the dynamics of water balance.

Consistent with the high correlation between SIF and TCI, variable importance from random forest regression also shows that temperature is the most important factor explaining the variance of SIF sensitivity to meteorological drought. Temperature has a significant positive correlation with $R_{SIF\text{-}SPEI05,}$ which means that there will be stronger SIF sensitivity to meteorological drought under higher temperature conditions. The reason could be that rising temperatures favorably influence vegetation activity and it is the main driver of many biological processes (such as enzyme-catalyzed reactions), which usually increase plant photosynthetic activity up to a certain point [*Badeck et al.*, 2004; *Karnieli et al.*, 2006]. It should be noted that those very high temperatures (>31.5 ^{o}C) decreases the sensitivity to meteorological drought (Figure 7). This is may be because vegetation under extremely high temperatures will decrease enzyme-catalyzed reactions and photosynthetic activity [*Mu et al.*, 2007; *Xiao et al.*, 2004; *Zhao et al.*, 2005].

It is worth noting that although SIF is less sensitive to precipitation than to temperature, precipitation is still a very important climate variable affecting SIF dynamics. There is a significant correlation between SIF and SPI, and including PET into SPEI does not significantly improve the correlation with SIF. The negative relationship between the $R_{SIF\text{-}SPEI05}$ and mean annual growing season precipitation (Figure 7) is similar to previous studies using other vegetation indices for drought monitoring. For example, *Vicente-Serrano* [2007] and *Quiring et al.* [2010] showed that the correlations between the *in-situ* meteorological drought index (SPI) and satellite-based vegetation condition index (VCI) are generally higher in dry locations than in wet regions. In our study, most of the high positive correlations between SIF and meteorological drought indices located in the dryland while most of the high negative correlations were in wet regions (Figures 1-3). It is likely because in drylands where precipitation is the dominant factor for vegetation growth, precipitation is a key important factor for determining the vegetation dynamics [*Wang et al.*, 2012], while in wet regions, additional precipitation does not change SIF signal significantly. In these regions, vegetation response to drought and moisture variations will be much more muted. In wet regions, there were more counties with significant negative r-values between SIF and TCI than between SIF and SPI (Figures 2-3). It may be because in wet regions, temperature other than precipitation is the dominant factor determining the vegetation dynamics.

4.2 SIF sensitivity to meteorological drought of different time scales and different ecosystem types

Our results indicate that different ecosystem types have different SIF sensitivity to meteorological drought. In this study, shrubland mainly refers to areas dominated by 5 m tall shrubs and young trees; grassland refers to areas dominated by grammanoid or herbaceous vegetation [*Homer et al.*, 2004]. Comparing with other ecosystems, shrubland, grassland, and cropland SIFs are more sensitive to short-term (1-month) meteorological drought indices, which indicates SIF could have fast response to meteorological drought for these ecosystem types. Grassland SIF only shows positive correlations to all the meteorological drought indices, which indicates decreasing of precipitation and increasing of temperature will decrease SIF values for grassland. The results also indicated that grassland SIF sensitivity does not significantly change for meteorological drought longer than 3-month time-scale. It means that grassland SIF will respond quite differently to 1-, 2-, and 3-month cumulative precipitation decrease or temperature increase but when the accumulation of precipitation decrease or temperature increase exceeds three months, grassland SIF will respond similarly. The positive correlation coefficients of cropland SIF and different time-scales of SPEI are similar to those between grassland SIF and SPEIs/SPIs. However, the negative correlation between cropland SIF and SPEI/SPIs indicates that meteorological drought could also increase crop SIF signal in some regions. Shrubland SIF generally has the highest positive correlation with all the meteorological drought indices across different time scales, and as the time-scale increase more counties have positive correlations. This indicates that shrubland SIF is also a fast response signal to meteorological drought conditions since it has high correlation with short-term SPI and SPEI (1-month time-scale). The negative correlation indicates that 1 to 7 month's cumulative decreasing precipitation or increasing temperature could increase SIF values for some regions. When the cumulative precipitation decrease or temperature increase exceeds 6 or 7 months, it only decreases shrub SIF signals, but the sensitivity of shrubland SIF to longer time-scale meteorological drought also decreases. It indicates that shrubland may have self-regulating strategies to alleviate SIF decrease under long-term meteorological drought (e.g., > 7-month). It also should be noted that there is a different pattern between the SIF-SPI relationship and SIF-SPEI relationship. There are higher positive r-values of wetland SIF and long-term SPEI (4-12 months) than the positive r-values of wetland SIF and long-term SPI (4-12 months). This is likely because in wetlands, the cumulative precipitation decrease is not the factor decreasing SIF signal and SIF signal

decrease is caused by the cumulative increase in potential evapotranspiration or high temperature beyond optimum vegetation growth threshold [*Huang et al.*, 2019; *Piao et al.*, 2014].

Spatially, the negative correlations in Pacific Northwest and Northeast regions are likely because these are wet regions and soil water is not limiting when meteorological drought occurs. Meteorological drought often occurs along with high temperature and low cloud cover, the increasing temperature and PAR during meteorological drought in these regions could increase satellite SIF values. It should be noted the heterogeneous pattern of the correlations in the Intermountain West may be due to data quality in this region. Due to the sparse coverage of vegetation in this region, there are many pixels without SIF data. Given the limited number of pixels in this region, the mean SIF pixel value of some counties may not reasonably reflect the large counties' value and therefore cause some statistical uncertainties. In this regard, the application of satellite SIF to meteorological drought response in this region should be treated with caution. The significant correlations in the middle regions of CONUS indicated that SIF signal in these regions has high sensitivity to meteorological drought.

Our results indicate that the overall correlations of SIF to 2-month time-scale of drought indices are significantly higher than the correlations between SIF and 1-month time-scale drought indices. The overall sensitivity of SIF to 3-month time-scale meteorological drought is slightly higher than to 2-month time-scale meteorological drought. The possible reason for the overall lower correlation between SIF and 1-month drought indices than with longer term drought indices is that vegetation growth is controlled by soil moisture and changes in vegetation growth signal are buffered by soil water storage [*Piao et al.*, 2003; *Quiring et al.*, 2010]. The occurrence of meteorological drought does not always mean plant water stress. For some regions when early meteorological droughts occur, vegetation could still have access to sufficient soil water to maintain functions without experiencing water stress for a period of time. In fact, the relationships between soil moisture and different time-scales of meteorological drought have been well documented. For example, *Wang et al.* [2015] indicated that there is a time-lag of soil moisture response to meteorological drought indices. It is shown that the SPEI of 1-3 month timescales has maximum correlations with soil moisture at soil depths of 0-5 cm, while SPEI of 9-12 month time scales has maximum correlations with soil moisture at soil depths of 90-100 cm.

4.3 Potential use of satellite SIF to study vegetation response to environmental stresses

Satellite SIF is an emerging satellite retrieval product, which could provide measurements closely or directly related to plant photosynthetic activity. There are growing interests to examine the effects of drought on SIF in recent years. Our research indicates that SIF is highly sensitive to temperature variation in the short time-scale (e.g., 1 month). The high SIF sensitivity to temperature indicates the potential use of SIF to monitor plant heat stress. Recently, *Song et al.* [2018] shows that SIF has the ability to detect winter wheat early response to heat stress in the Indian Indo-Gangetic Plains when comparing with NDVI and EVI. Future research could focus on SIF sensitivities to heat stress over regional to global scales and explore the mechanisms of plant functions involving heat stress. In addition, because SIF has high sensitivity to temperature variations it has potential to investigate changes in plant photosynthetic activity under global warming. This is important because there are uncertainties using existing VIs to evaluate plant photosynthetic activity responses to warming due to saturation issue, background effect or sensor degradation [*Gao et al.*, 2000; *Nicholson et al.*, 1994; *Zhang et al.*, 2017].

With growing interests in satellite SIF, more satellite products at regional to global scale will become available such as TROPOMI SIF product with a global coverage [*Köhler et al.*, 2018]. Future study can also take advantage of satellite SIF products extracted from satellite observation models such as high resolution global contiguous OCO-2 based SIF product [*Yu et al.*, 2018]. In this study, we compared the original GOME-2 SIF product and downscaled high spatial resolution GOME-2 SIF product by [*Duveiller et al.*, 2016], they showed a similar pattern when correlated to the meteorological drought indices (Figures S7-S9).

Our research analyzed the characteristics of SIF responses to meteorological drought. However, it should be noted that several factors could potentially affect the sensitivity analysis of SIF to meteorological drought. Firstly, we assessed the sensitivity of SIF to meteorological drought based on the Spearman rank correlation analysis between SIF anomalies and meteorological drought indices. However, correlation does not always imply causation. Ground-based SIF measurements would be valuable to examine the mechanisms in the future. In addition, this study analyzed data at the county level. Small counties may be smaller than the smallest SIF grid cell, and large counties in the west may contain multiple SIF grid cells. This may add uncertainties to our evaluation results. At the same time,

political boundaries, in general, and county boundaries, in particular, are commonly used for making drought-related decisions.

5 Conclusions

This study examines the spatial relationship between satellite SIF and four commonly used meteorological drought indices of different time-scales in different climate regions across the CONUS. We found that satellite SIF is more sensitive to meteorological drought through temperature effect than through precipitation and potential evapotranspiration effects. We also demonstrate that the sensitivity of satellite SIF response to meteorological drought varies significantly in different climate regions and for different ecosystem types. Grassland and shrubland SIF show higher sensitivity to meteorological drought than other ecosystem types. Grassland SIF responds quite differently to 1-, 2-, and 3-month cumulative precipitation decrease or temperature increase. However, when the accumulation of precipitation decrease or temperature exceeds three months, SIF responds similarly. SIF is sensitive to meteorological drought only in climate regions with high growing season temperature, low growing season precipitation and low GPP. Among the environmental variables, mean annual growing season temperature is the most important determinant for the sensitivity of satellite SIF to meteorological drought.

Acknowledgments

We acknowledge support from Division of Earth Sciences of National Science Foundation (NSF EAR-1554894) and from the Agriculture and Food Research Initiative program (2017-67013-26191) of the USDA National Institute of Food and Agriculture. All the data used in this study is discussed in Section 2 Data and Methodology. There is no additional data to declare.

6 References

AghaKouchak, A., A. Farahmand, F. Melton, J. Teixeira, M. Anderson, B. D. Wardlow, and C. Hain (2015), Remote sensing of drought: Progress, challenges and opportunities, *Reviews of Geophysics*, *53*(2), 452-480.

Anderegg, W. R., A. G. Konings, A. T. Trugman, K. Yu, D. R. Bowling, R. Gabbitas, D. S. Karp, S. Pacala, J. S. Sperry, and B. N. Sulman (2018), Hydraulic diversity of forests regulates ecosystem resilience during drought, *Nature*, *561*(7724), 538.

Asner, G. P., and A. Alencar (2010), Drought impacts on the Amazon forest: the remote sensing perspective, *New Phytologist*, *187*(3), 569-578.

Badeck, F. W., A. Bondeau, K. Böttcher, D. Doktor, W. Lucht, J. Schaber, and S. Sitch (2004), Responses of spring phenology to climate change, *New Phytologist*, *162*(2), 295-309.

Banimahd, S. A., and D. Khalili (2013), Factors influencing Markov chains predictability characteristics, utilizing SPI, RDI, EDI and SPEI drought indices in different climatic zones, *Water Resources Management*, *27*(11), 3911-3928.

Bhuiyan, C., R. Singh, and F. N. Kogan (2006), Monitoring drought dynamics in the Aravalli region (India) using different indices based on ground and remote sensing data, *International Journal of Applied Earth Observation and Geoinformation*, *8*(4), 289-302.

Breiman, L. (1996), Out-of-bag estimation, edited, Citeseer.

Breiman, L. (2001), Random forests, *Machine Learning*, *45*(1), 5-32.

Chang, Q., J. Zhang, W. Jiao, and F. Yao (2018), A comparative analysis of the NDVIg and NDVI3g in monitoring vegetation phenology changes in the Northern Hemisphere, *Geocarto International*, *33*(1), 1-20.

Dai, A. (2011), Drought under global warming: a review, *Wiley Interdisciplinary Reviews: Climate Change*, *2*(1), 45-65.

Damm, A., J. Elbers, A. Erler, B. Gioli, K. Hamdi, R. Hutjes, M. Kosvancova, M. Meroni, F. Miglietta, and A. Moersch (2010), Remote sensing of sun-induced fluorescence to improve

modeling of diurnal courses of gross primary production. , *Global Change Biology*, *16*(1), 171-186.

Di, L., D. C. Rundquist, and L. Han (1994), Modelling relationships between NDVI and precipitation during vegetative growth cycles, *International Journal of Remote Sensing*, *15*(10), 2121-2136.

Dobrowski, S., J. Pushnik, P. Zarco-Tejada, and S. Ustin (2005), Simple reflectance indices track heat and water stress-induced changes in steady-state chlorophyll fluorescence at the canopy scale, *Remote Sensing of Environment*, *97*(3), 403-414.

Duveiller, G., and A. Cescatti (2016), Spatially downscaling sun-induced chlorophyll fluorescence leads to an improved temporal correlation with gross primary productivity, *Remote Sensing of Environment*, *182*, 72-89.

Frankenberg, C., J. B. Fisher, J. Worden, G. Badgley, S. S. Saatchi, J. E. Lee, G. C. Toon, A. Butz, M. Jung, and A. Kuze (2011), New global observations of the terrestrial carbon cycle from GOSAT: Patterns of plant fluorescence with gross primary productivity, *Geophysical Research Letters*, *38*(17).

Frankenberg, C., C. O'Dell, J. Berry, L. Guanter, J. Joiner, P. Köhler, R. Pollock, and T. E. Taylor (2014), Prospects for chlorophyll fluorescence remote sensing from the Orbiting Carbon Observatory-2, *Remote Sensing of Environment*, *147*, 1-12.

Gao, X., A. R. Huete, W. Ni, and T. Miura (2000), Optical–biophysical relationships of vegetation spectra without background contamination, *Remote Sensing of Environment*, *74*(3), 609-620.

Griffin, D., and K. J. Anchukaitis (2014), How unusual is the 2012–2014 California drought?, *Geophysical Research Letters*, *41*(24), 9017-9023.

Griggs, D. J., and M. Noguer (2002), Climate change 2001: the scientific basis. Contribution of working group I to the third assessment report of the intergovernmental panel on climate change, *Weather*, *57*(8), 267-269.

Guan, K., J. A. Berry, Y. Zhang, J. Joiner, L. Guanter, G. Badgley, and D. B. Lobell (2016), Improving the monitoring of crop productivity using spaceborne solar-induced fluorescence, *Global Change Biology*, *22*(2), 716-726.

Guanter, L., L. Alonso, L. Gómez-Chova, J. Amorós-López, J. Vila, and J. Moreno (2007), Estimation of solar-induced vegetation fluorescence from space measurements, *Geophysical Research Letters*, *34*(8).

Guanter, L., C. Frankenberg, A. Dudhia, P. E. Lewis, J. Gómez-Dans, A. Kuze, H. Suto, and R. G. Grainger (2012), Retrieval and global assessment of terrestrial chlorophyll fluorescence from GOSAT space measurements, *Remote Sensing of Environment*, *121*, 236-251.

Guanter, L., P. Köhler, S. Walther, and Y. Zhang (2016), Recent advances in global monitoring of terrestrial sun-induced chlorophyll fluorescence, paper presented at Geoscience and Remote Sensing Symposium (IGARSS), 2016 IEEE International, IEEE.

Guanter, L., Y. Zhang, M. Jung, J. Joiner, M. Voigt, J. A. Berry, C. Frankenberg, A. R. Huete, P. Zarco-Tejada, and J.-E. Lee (2014), Reply to Magnani et al.: Linking large-scale chlorophyll fluorescence observations with cropland gross primary production, *Proceedings of the National Academy of Sciences*, *111*(25), E2511-E2511.

Hao, C., J. Zhang, and F. Yao (2015), Combination of multi-sensor remote sensing data for drought monitoring over Southwest China, *International Journal of Applied Earth Observation and Geoinformation*, *35*, 270-283.

Hao, Z., A. AghaKouchak, N. Nakhjiri, and A. Farahmand (2014), Global integrated drought monitoring and prediction system, *Scientific Data*, *1*, 140001.

Hao, Z., and V. P. Singh (2015), Drought characterization from a multivariate perspective: A review, *Journal of Hydrology*, *527*, 668-678, doi:http://dx.doi.org/10.1016/j.jhydrol.2015.05.031.

Hao, Z., X. Yuan, Y. Xia, F. Hao, and V. P. Singh (2017), An overview of drought monitoring and prediction systems at regional and global scales, *Bulletin of the American Meteorological Society*, *98*(9), 1879-1896.

Hayes, M. J., M. D. Svoboda, D. A. Wilhite, and O. V. Vanyarkho (1999), Monitoring the 1996 drought using the standardized precipitation index, *Bulletin of the American Meteorological Society*, *80*(3), 429-438.

Homer, C., C. Huang, L. Yang, B. Wylie, and M. Coan (2004), Development of a 2001 national land-cover database for the United States, *Photogrammetric Engineering & Remote Sensing*, *70*(7), 829-840.

Huang, M., S. Piao, P. Ciais, J. Peñuelas, X. Wang, T. F. Keenan, S. Peng, J. A. Berry, K. Wang, and J. Mao (2019), Air temperature optima of vegetation productivity across global biomes, *Nature ecology & evolution*, 1.

Ishwaran, H. (2007), Variable importance in binary regression trees and forests, *Electronic Journal of Statistics*, *1*, 519-537.

Ji, L., and A. J. Peters (2003), Assessing vegetation response to drought in the northern Great Plains using vegetation and drought indices, *Remote Sensing of Environment*, *87*(1), 85-98, doi:https://doi.org/10.1016/S0034-4257(03)00174-3.

Jiao, W., C. Tian, Q. Chang, K. A. Novick, and L. Wang (2019), A new multi-sensor integrated index for drought monitoring, *Agricultural and Forest Meteorology*, *268*, 74-85, doi:https://doi.org/10.1016/j.agrformet.2019.01.008.

Jiao, W., L. Zhang, Q. Chang, D. Fu, Y. Cen, and Q. Tong (2016), Evaluating an enhanced vegetation condition index based on VIUPD for drought monitoring in the continental United States, *Remote Sensing*, *8*(3), 224.

Joiner, J., L. Guanter, R. Lindstrot, M. Voigt, A. Vasilkov, E. Middleton, K. Huemmrich, Y. Yoshida, and C. Frankenberg (2013), Global monitoring of terrestrial chlorophyll fluorescence from moderate spectral resolution near-infrared satellite measurements: methodology, simulations, and application to GOME-2, *Atmospheric Measurement Techniques*, *6*(2), 2803-2823.

Joiner, J., Y. Yoshida, A. Vasilkov, and E. Middleton (2011), First observations of global and seasonal terrestrial chlorophyll fluorescence from space, *Biogeosciences*, *8*(3), 637-651.

Karnieli, A., M. Bayasgalan, Y. Bayarjargal, N. Agam, S. Khudulmur, and C. Tucker (2006), Comments on the use of the vegetation health index over Mongolia, *International Journal of Remote Sensing*, *27*(10), 2017-2024.

Keeley, J. E., H. Safford, C. Fotheringham, J. Franklin, and M. Moritz (2009), The 2007 southern California wildfires: lessons in complexity, *Journal of Forestry*, *107*(6), 287-296.

Kogan, F. (1995), Application of vegetation index and brightness temperature for drought detection, *Advances in Space Research*, *15*(11), 91-100.

Kogan, F. N. (1997), Global drought watch from space, *Bulletin of the American Meteorological Society*, *78*(4), 621-636.

Köhler, P., C. Frankenberg, T. S. Magney, L. Guanter, J. Joiner, and J. Landgraf (2018), Global Retrievals of Solar-Induced Chlorophyll Fluorescence With TROPOMI: First Results and Intersensor Comparison to OCO-2, *Geophysical Research Letters*, *45*(19), 10,456-410,463.

Köhler, P., L. Guanter, and J. Joiner (2015), A linear method for the retrieval of sun-induced chlorophyll fluorescence from GOME-2 and SCIAMACHY data, *Atmospheric Measurement Techniques*, *8*(6), 2589-2608.

Liu, L., and Z. Cheng (2010), Detection of vegetation light-use efficiency based on solar-induced chlorophyll fluorescence separated from canopy radiance spectrum, *IEEE Journal of Selected Topics in Applied Earth Observations and Remote Sensing*, *3*(3), 306-312.

Liu, L., X. Yang, H. Zhou, S. Liu, L. Zhou, X. Li, J. Yang, X. Han, and J. Wu (2018a), Evaluating the utility of solar-induced chlorophyll fluorescence for drought monitoring by comparison with NDVI derived from wheat canopy, *Science of The Total Environment*, *625*, 1208-1217, doi:https://doi.org/10.1016/j.scitotenv.2017.12.268.

Liu, L., X. Yang, H. Zhou, S. Liu, L. Zhou, X. Li, J. Yang, and J. Wu (2018b), Relationship of root zone soil moisture with solar-induced chlorophyll fluorescence and vegetation indices in winter wheat: A comparative study based on continuous ground-measurements, *Ecological Indicators*, *90*, 9-17.

Liu, W., and F. Kogan (1996), Monitoring regional drought using the vegetation condition index, *International Journal of Remote Sensing*, *17*(14), 2761-2782.

McKee, T. B., N. J. Doesken, and J. Kleist (1993), The relationship of drought frequency and duration to time scales, paper presented at Proceedings of the 8th Conference on Applied Climatology, American Meteorological Society Boston, MA.

Meroni, M., M. Rossini, L. Guanter, L. Alonso, U. Rascher, R. Colombo, and J. Moreno (2009), Remote sensing of solar-induced chlorophyll fluorescence: Review of methods and applications, *Remote Sensing of Environment*, *113*(10), 2037-2051.

Mishra, A. K., and V. P. Singh (2010), A review of drought concepts, *Journal of Hydrology*, *391*(1), 202-216.

Mu, Q., F. A. Heinsch, M. Zhao, and S. W. Running (2007), Development of a global evapotranspiration algorithm based on MODIS and global meteorology data, *Remote Sensing of Environment*, *111*(4), 519-536.

Myneni, R. B., J. Ross, and G. Asrar (1989), A review on the theory of photon transport in leaf canopies, *Agricultural and Forest Meteorology*, *45*(1-2), 1-153.

Neitsch, S. L., J. G. Arnold, J. R. Kiniry, and J. R. Williams (2011), Soil and water assessment tool theoretical documentation version 2009*Rep.*, Texas Water Resources Institute.

Nicholson, S., and T. Farrar (1994), The influence of soil type on the relationships between NDVI, rainfall, and soil moisture in semiarid Botswana. I. NDVI response to rainfall, *Remote Sensing of Environment*, *50*(2), 107-120.

Nielsen-Gammon, J. (2011), The 2011 Texas drought: a briefing packet for the Texas Legislature*Rep.*

Palmer, W. C. (1965), *Meteorological drought*, Citeseer.

Pérez‐Priego, O., J.-H. Guan, M. Rossini, F. Fava, T. Wutzler, G. Moreno, N. Carvalhais, A. Carrara, O. Kolle, and T. Julitta (2015), Sun-induced chlorophyll fluorescence and photochemical reflectance index improve remote-sensing gross primary production estimates under varying nutrient availability in a typical Mediterranean savanna ecosystem, *Biogeosciences*, *12*(21), 6351-6367.

Piao, S., J. Fang, L. Zhou, Q. Guo, M. Henderson, W. Ji, Y. Li, and S. Tao (2003), Interannual variations of monthly and seasonal normalized difference vegetation index (NDVI) in China from 1982 to 1999, *Journal of Geophysical Research: Atmospheres*, *108*(D14).

Piao, S., H. Nan, C. Huntingford, P. Ciais, P. Friedlingstein, S. Sitch, S. Peng, A. Ahlström, J. G. Canadell, and N. Cong (2014), Evidence for a weakening relationship between interannual temperature variability and northern vegetation activity, *Nature communications*, *5*, 5018.

Porcar-Castell, A., E. Tyystjärvi, J. Atherton, C. van der Tol, J. Flexas, E. E. Pfündel, J. Moreno, C. Frankenberg, and J. A. Berry (2014), Linking chlorophyll a fluorescence to photosynthesis for remote sensing applications: mechanisms and challenges, *Journal of Experimental Botany*, *65*(15), 4065-4095.

Quiring, S. M., and S. Ganesh (2010), Evaluating the utility of the Vegetation Condition Index (VCI) for monitoring meteorological drought in Texas, *Agricultural and Forest Meteorology*, *150*(3), 330-339.

Rajsekhar, D., V. P. Singh, and A. K. Mishra (2015), Multivariate drought index: An information theory based approach for integrated drought assessment, *Journal of Hydrology*, *526*, 164-182.

Rhee, J., J. Im, and G. J. Carbone (2010), Monitoring agricultural drought for arid and humid regions using multi-sensor remote sensing data, *Remote Sensing of Environment*, *114*(12), 2875-2887.

Sheffield, J., E. F. Wood, and M. L. Roderick (2012), Little change in global drought over the past 60 years, *Nature*, *491*(7424), 435-438.

Singh, R. P., S. Roy, and F. Kogan (2003), Vegetation and temperature condition indices from NOAA AVHRR data for drought monitoring over India, *International Journal of Remote Sensing*, *24*(22), 4393-4402.

Song, L., L. Guanter, K. Guan, L. You, A. Huete, W. Ju, and Y. Zhang (2018), Satellite sun-induced chlorophyll fluorescence detects early response of winter wheat to heat stress in the Indian Indo-Gangetic Plains, *Global change biology*.

Sun, Y., C. Frankenberg, M. Jung, J. Joiner, L. Guanter, P. Köhler, and T. Magney (2018), Overview of Solar-Induced chlorophyll Fluorescence (SIF) from the Orbiting Carbon Observatory-2: Retrieval, cross-mission comparison, and global monitoring for GPP, *Remote Sensing of Environment*, *209*, 808-823.

Sun, Y., R. Fu, R. Dickinson, J. Joiner, C. Frankenberg, L. Gu, Y. Xia, and N. Fernando (2015), Drought onset mechanisms revealed by satellite solar-induced chlorophyll fluorescence: Insights from two contrasting extreme events, *Journal of Geophysical Research: Biogeosciences*, *120*(11), 2427-2440.

Tate, E., and A. Gustard (2000), Drought definition: a hydrological perspective, in *Drought and drought mitigation in Europe*, edited, pp. 23-48, Springer.

Tucker, C. J., and B. J. Choudhury (1987), Satellite remote sensing of drought conditions, *Remote Sensing of Environment*, *23*(2), 243-251.

Unganai, L. S., and F. N. Kogan (1998), Drought monitoring and corn yield estimation in Southern Africa from AVHRR data, *Remote Sensing of Environment*, *63*(3), 219-232.

Van Loon, A. F., K. Stahl, G. Di Baldassarre, J. Clark, S. Rangecroft, N. Wanders, T. Gleeson, A. I. Van Dijk, L. M. Tallaksen, and J. Hannaford (2016), Drought in a human-modified world: reframing drought definitions, understanding, and analysis approaches, *Hydrology and Earth System Sciences*, *20*(9), 3631.

Vicente-Serrano, S. M. (2007), Evaluating the impact of drought using remote sensing in a Mediterranean, semi-arid region, *Natural Hazards*, *40*(1), 173-208.

Vicente-Serrano, S. M., S. Beguería, and J. I. López-Moreno (2010), A multiscalar drought index sensitive to global warming: the standardized precipitation evapotranspiration index, *Journal of Climate*, *23*(7), 1696-1718.

Vicente-Serrano, S. M., C. Gouveia, J. J. Camarero, S. Beguería, R. Trigo, J. I. López-Moreno, C. Azorín-Molina, E. Pasho, J. Lorenzo-Lacruz, and J. Revuelto (2013), Response of vegetation to drought time-scales across global land biomes, *Proceedings of the National Academy of Sciences*, *110*(1), 52-57.

Wang, H., B. He, Y. Zhang, L. Huang, Z. Chen, and J. Liu (2018), Response of ecosystem productivity to dry/wet conditions indicated by different drought indices, *Science of The Total Environment*, *612*, 347-357.

Wang, H., J. C. Rogers, and D. K. Munroe (2015), Commonly used drought indices as indicators of soil moisture in China, *Journal of Hydrometeorology*, *16*(3), 1397-1408.

Wang, L., P. d'Odorico, J. Evans, D. Eldridge, M. McCabe, K. Caylor, and E. King (2012), Dryland ecohydrology and climate change: critical issues and technical advances, *Hydrology and Earth System Sciences*, *16*(8), 2585.

Wang, S., C. Huang, L. Zhang, Y. Lin, Y. Cen, and T. Wu (2016), Monitoring and assessing the 2012 drought in the great plains: Analyzing satellite-retrieved solar-induced chlorophyll fluorescence, drought indices, and gross primary production, *Remote Sensing*, *8*(2), 61.

Williams, A. P., R. Seager, J. T. Abatzoglou, B. I. Cook, J. E. Smerdon, and E. R. Cook (2015), Contribution of anthropogenic warming to California drought during 2012–2014, *Geophysical Research Letters*, *42*(16), 6819-6828.

Xiao, X., D. Hollinger, J. Aber, M. Goltz, E. A. Davidson, Q. Zhang, and B. Moore III (2004), Satellite-based modeling of gross primary production in an evergreen needleleaf forest, *Remote Sensing of Environment*, *89*(4), 519-534.

Yang, X., J. Tang, J. F. Mustard, J. E. Lee, M. Rossini, J. Joiner, J. W. Munger, A. Kornfeld, and A. D. Richardson (2015), Solar-induced chlorophyll fluorescence that correlates with canopy photosynthesis on diurnal and seasonal scales in a temperate deciduous forest, *Geophysical Research Letters*, *42*(8), 2977-2987.

Yoshida, Y., J. Joiner, C. Tucker, J. Berry, J.-E. Lee, G. Walker, R. Reichle, R. Koster, A. Lyapustin, and Y. Wang (2015), The 2010 Russian drought impact on satellite measurements of solar-induced chlorophyll fluorescence: Insights from modeling and comparisons with parameters derived from satellite reflectances, *Remote Sensing of Environment*, *166*, 163-177.

Yu, L., J. Wen, C. Y. Chang, C. Frankenberg, and Y. Sun (2018), High Resolution Global Contiguous Solar-Induced Chlorophyll Fluorescence (SIF) of Orbiting Carbon Observatory-2 (OCO-2), *Geophysical Research Letters*, *0*(ja), doi:doi:10.1029/2018GL081109.

Zhang, L., W. Jiao, H. Zhang, C. Huang, and Q. Tong (2017), Studying drought phenomena in the Continental United States in 2011 and 2012 using various drought indices, *Remote Sensing of Environment*, *190*, 96-106.

Zhang, Y., C. Song, L. E. Band, G. Sun, and J. Li (2017), Reanalysis of global terrestrial vegetation trends from MODIS products: Browning or greening?, *Remote Sensing of Environment*, *191*, 145-155.

Zhao, H., G. Gao, W. An, X. Zou, H. Li, and M. Hou (2017), Timescale differences between SC-PDSI and SPEI for drought monitoring in China, *Physics and Chemistry of the Earth, Parts A/B/C*, *102*, 48-58.

Zhao, M., F. A. Heinsch, R. R. Nemani, and S. W. Running (2005), Improvements of the MODIS terrestrial gross and net primary production global data set, *Remote Sensing of Environment*, *95*(2), 164-176.

Zhou, L., J. Zhang, J. Wu, L. Zhao, M. Liu, A. Lü, and Z. Wu (2012), Comparison of remotely sensed and meteorological data-derived drought indices in mid-eastern China, *International Journal of Remote Sensing*, *33*(6), 1755-1779.

Table 1 Summary of the meteorological drought indices used in this study.

Drought index	Required metrological factors	Method	Source
SPI	Precipitation	Based on the historical precipitation occurrence probability distribution function	[*McKee et al.*, 1993]
SPEI	Potential evapotranspiration and precipitation	Based on the historical deficiency of precipitation (P-PET) occurrence probability distribution function	[*Vicente-Serrano et al.*, 2010]
TCI	Land surface temperature (LST)	Based on LST anomaly	[*Kogan*, 1997]
PDSI	Precipitation, temperature, and potential evapotranspiration	Based on water balance model	[*Palmer*, 1965]

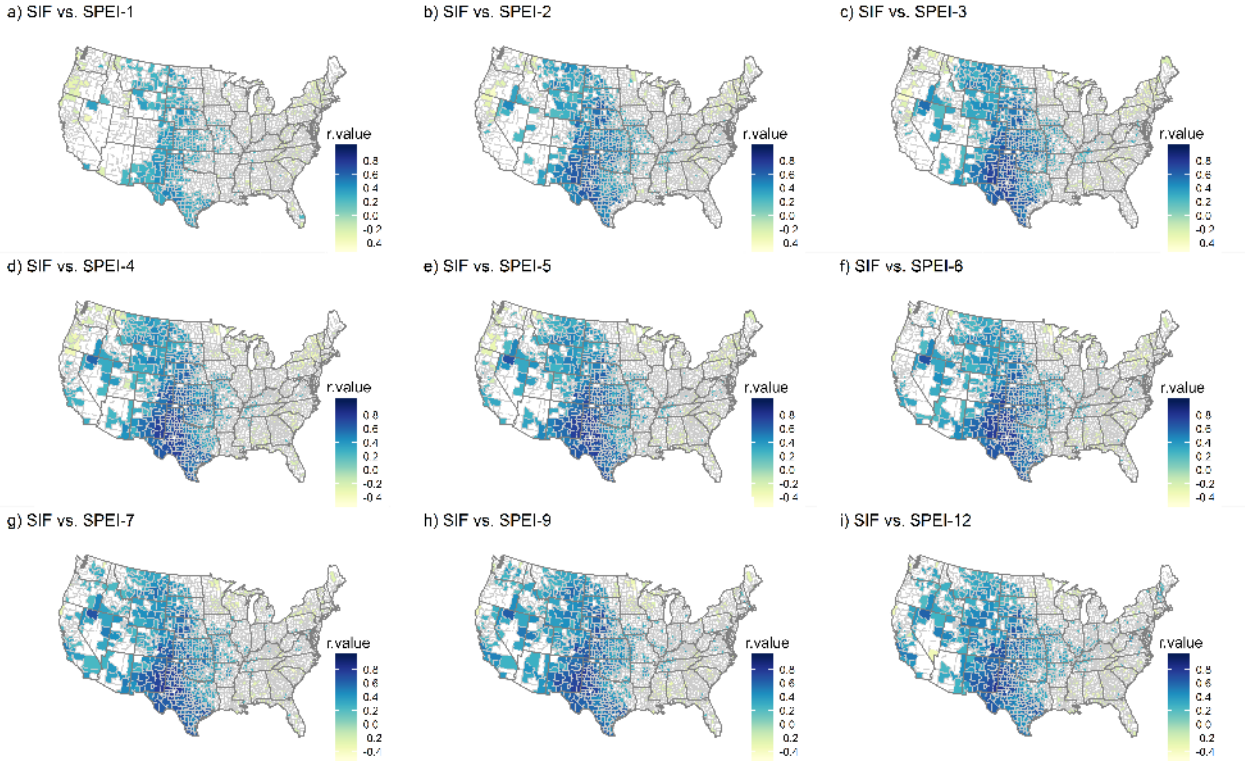

Figure 1. Spatial variations of the r-values between SIF and SPEI at 1-month (a), 2-month (b), 3-month (c), 4-month (d), 5-month (e), 6-month (f), 7-month (g), 9-month (h), 12-month (i) time scale. Counties with white color means insignificant correlations (p-value > 0.05) in those counties.

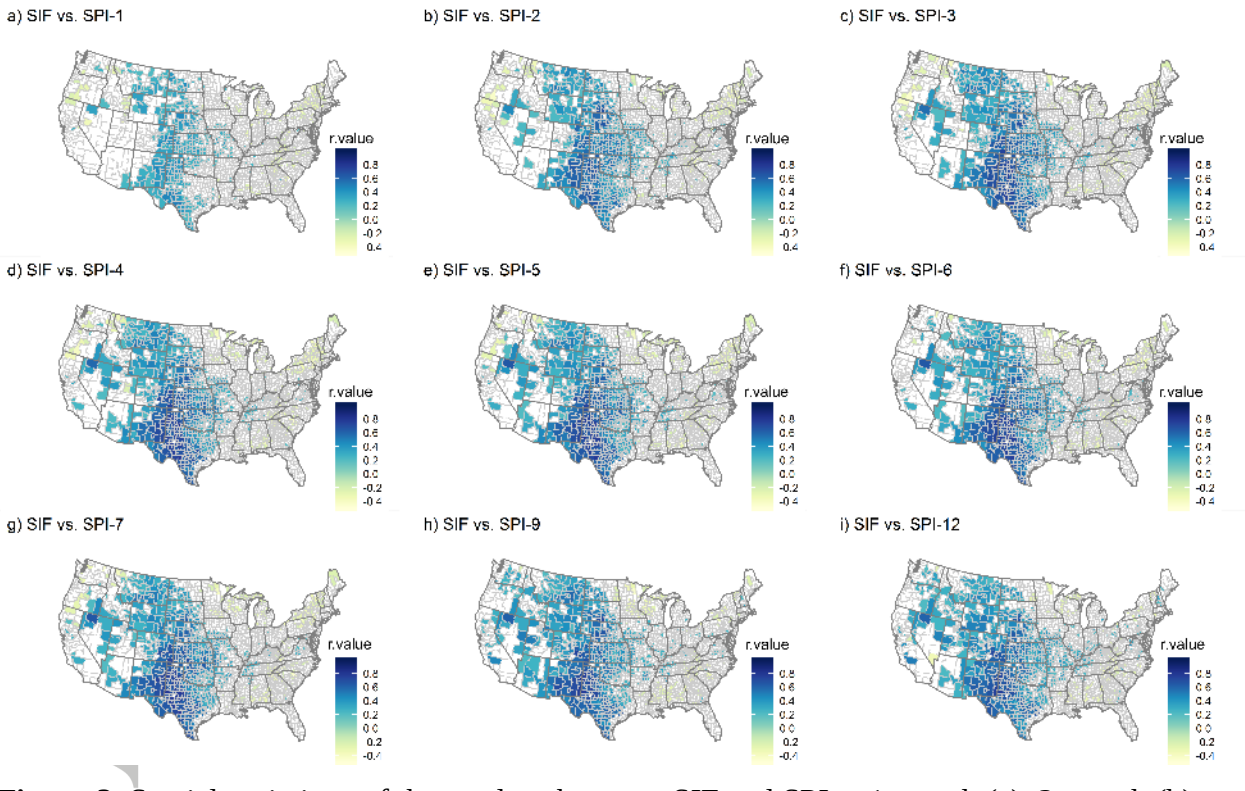

Figure 2. Spatial variations of the r-values between SIF and SPI at 1-month (a), 2-month (b), 3-month (c), 4-month (d), 5-month (e), 6-month (f), 7-month (g), 9-month (h), 12-month (i) time scale. Counties with white color means insignificant correlations (p-value > 0.05) in those counties.

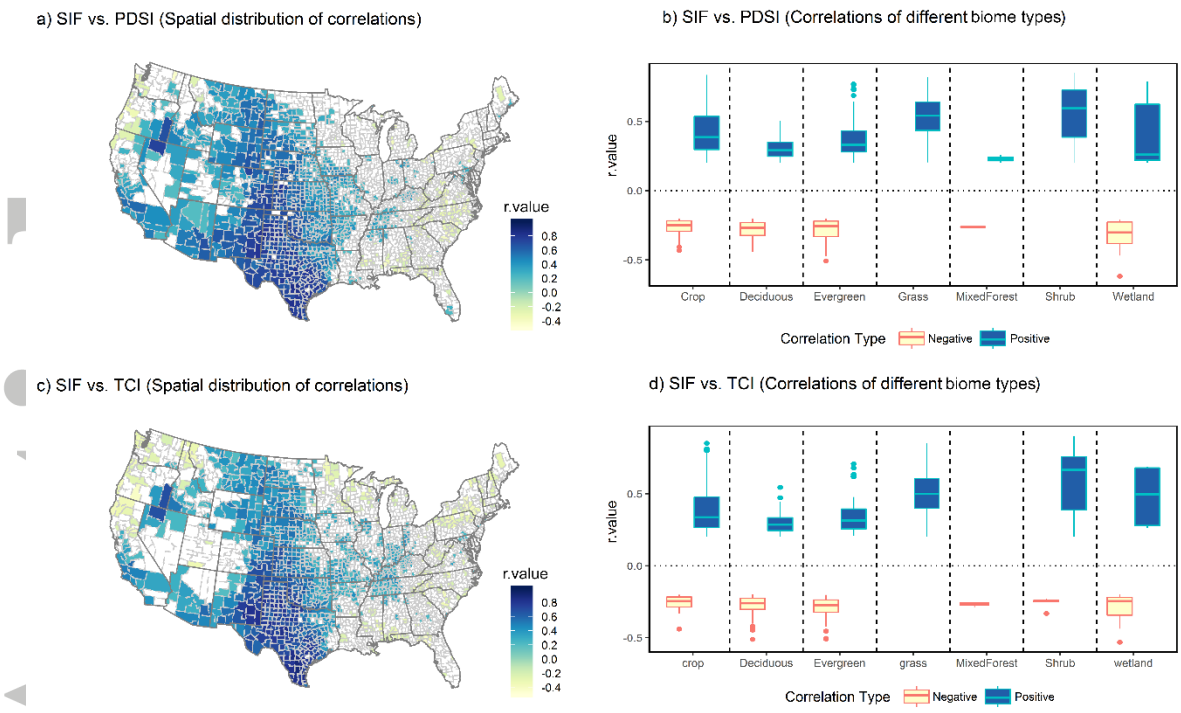

Figure 3. Spatial variations of the r-values between SIF and PDSI (a) as well as between SIF and TCI (c). Counties with white color means insignificant correlations (p-values > 0.05) in those counties. The correlations (r-value) between SIF and PDSI (b) as well as between SIF and TCI (d) for different ecosystem types. All the reported correlation coefficients are statistically significant.

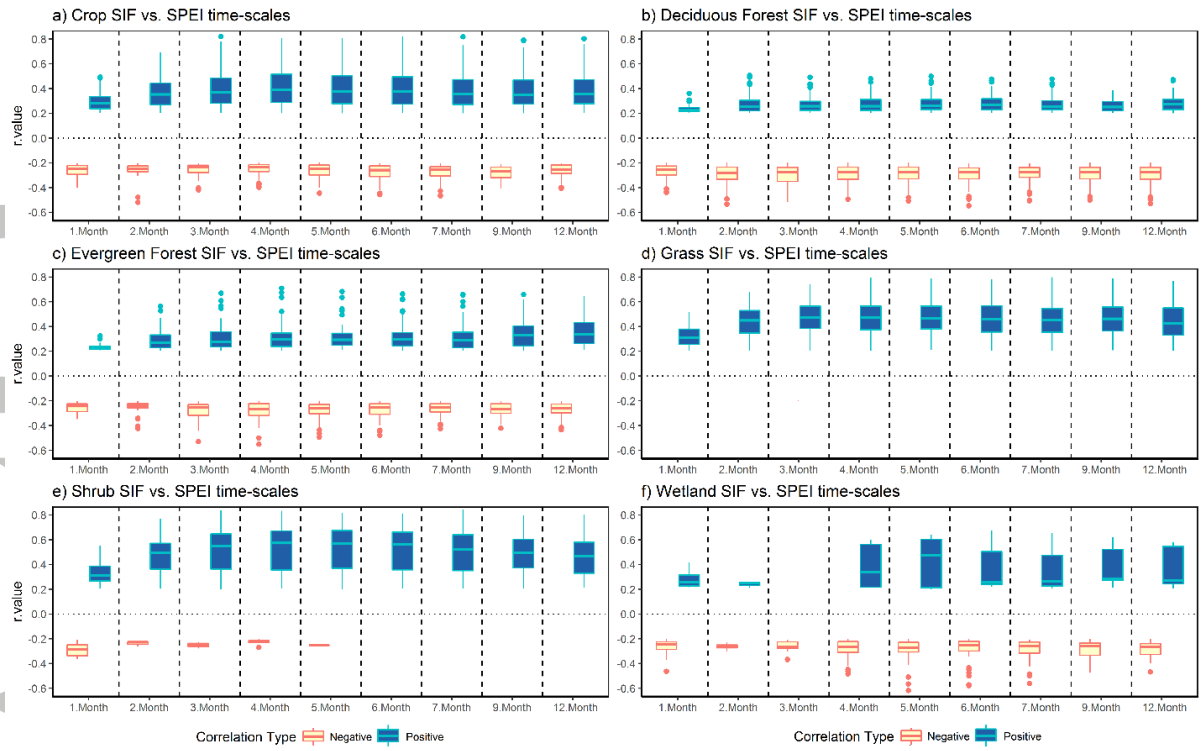

Figure 4. The correlations (r-value) between SIF and SPEI under different time-scales for the ecosystem types of Cropland (a), deciduous forest (b), evergreen forest (c), Grassland (d), shrubland (e), and wetland (f). All the reported correlation coefficients are statistically significant.

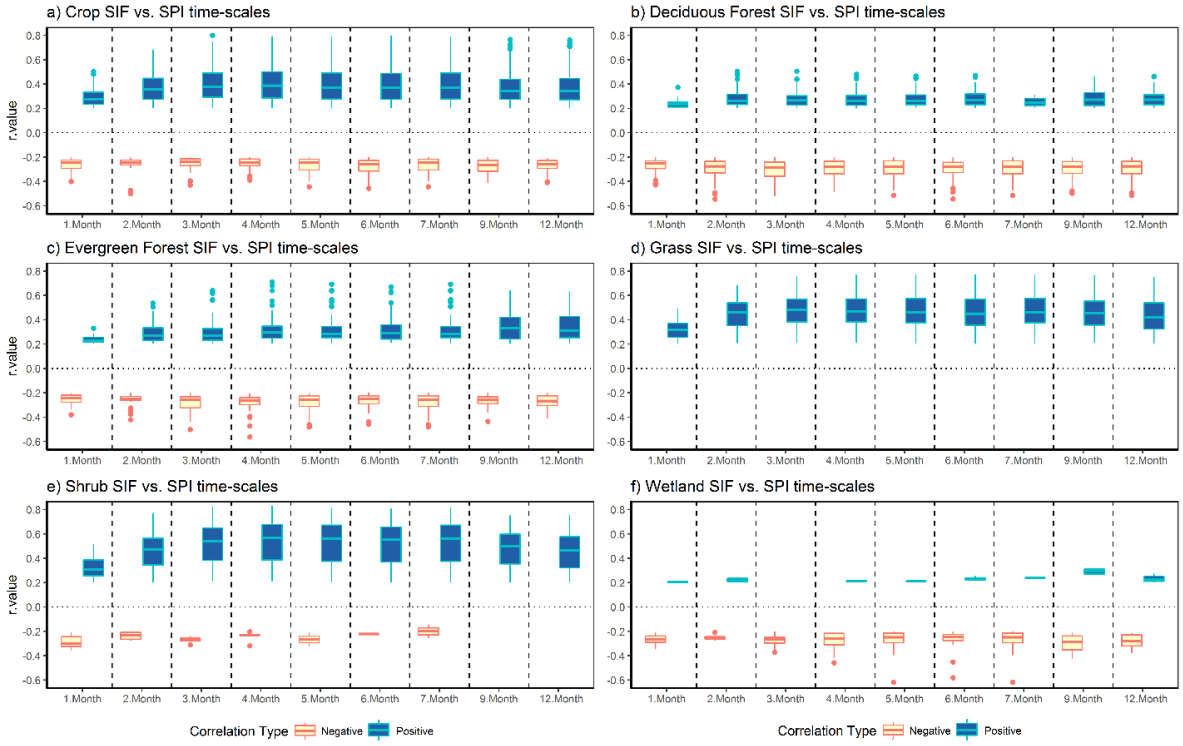

Figure 5. The correlations (r-value) between SIF and SPI under different time-scales for the ecosystem types of cropland (a), deciduous forest (b), evergreen forest (c), grassland (d), shrubland (e), and wetland (f). All the reported correlation coefficients are statistically significant.

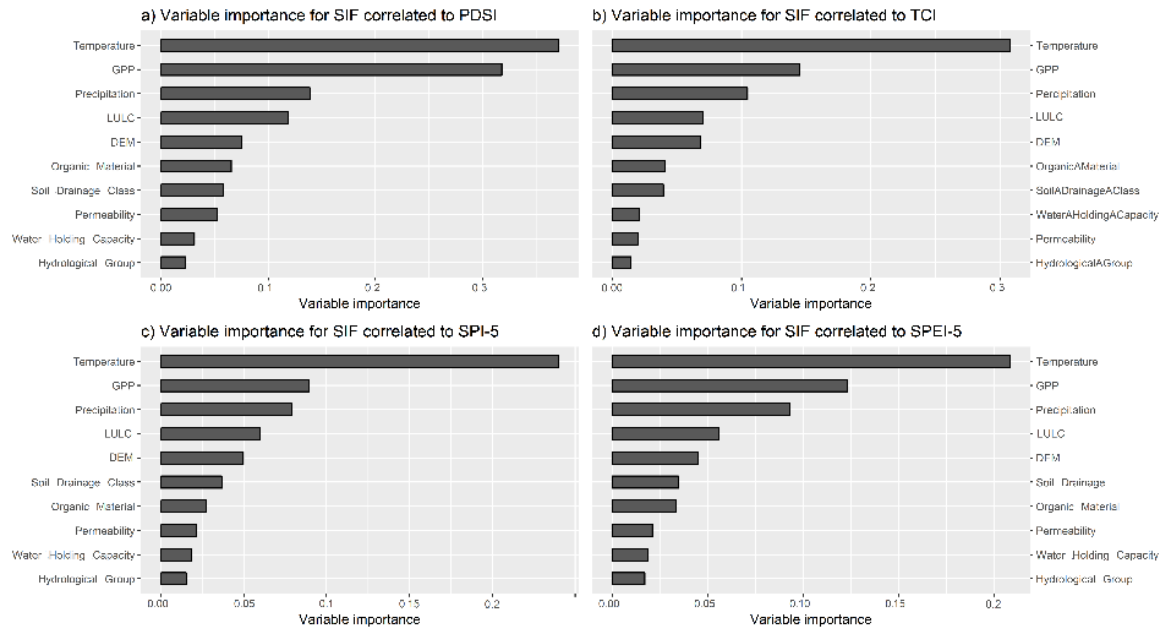

Figure 6. Variable importance of ten environmental variables for explaining the relationship between SIF anomaly and meteorological drought indices (SPEI, SPI, TCI and PDSI).

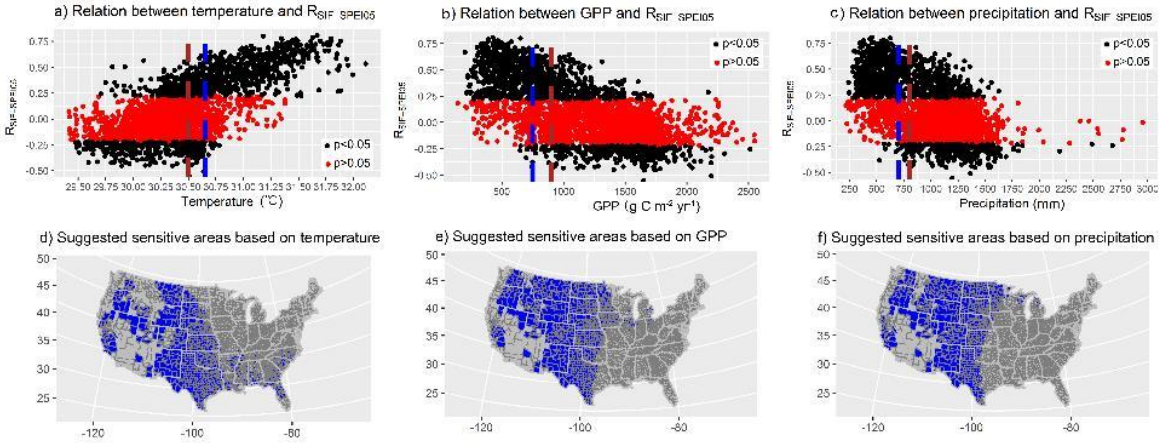

Figure 7. The dependence of SIF and 5-month SPEI correlation ($R_{SIF\text{-}SPEI05}$) on mean annual temperature (a), GPP (b) and precipitation (c). The blue and brown lines represent the thresholds of 90% and 80% of the counties with significant relationship between SIF and SPEI, respectively. The blue colored regions represent the areas meet the 80% threshold regarding temperature (d), GPP (e) and precipitation (f) for SIF being sensitive to meteorological drought. Red points in (a)-(c) represent the counties with non-significant relationships between SIF and SPEI-5 ($p>0.05$) and black points represent counties with significant correlations ($p<0.05$).